**Article:**

Hepburn, A.J., Ng, F.S.L. orcid.org/0000-0001-6352-0351, Livingstone, S.J. et al. (2 more authors) (2020) Polyphase mid-latitude glaciation on Mars: chronology of the formation of superposed glacier-like forms from crater-count dating. Journal of Geophysical Research: Planets, 125 (2). e2019JE006102. ISSN 2169-9100

https://doi.org/10.1029/2019JE006102

# Supporting Information for "Polyphase mid-latitude glaciation on Mars: chronology of the formation of superposed glacier-like forms from crater-count dating"

**A.J. Hepburn[1,2], F.S.L. Ng[2], S.J. Livingstone[2], T.O.Holt[1], B.Hubbard[1]**

[1]Department of Geography and Earth Sciences, Aberystwyth University, Aberystwyth SY23 3DB, UK

[2]Department of Geography, University of Sheffield, Sheffield S10 2TN, UK

**Contents of this file:**



Movie S1 (separate file in .MP4 format). **Formation sequence of superposed glacier like forms (SGLFs) and their underlying viscous flow features (underlying VFFs) from 300 Ma to today.** Background shows MOLA gridded topography in cylindrical projection. (**A**) covers the globe. (**B**) and (**C**) expand the regions of Deuteronilus-Protonilus Mensae and Eastern Hellas. Two phases of glacier recession, R2 and R1, are portrayed by the intense production of new SGLFs (red points) in 45-65 Ma and 2-20 Ma, respec-

Corresponding author: A.J. Hepburn, adh28@aber.ac.uk

Corresponding author: F.S.L. Ng, f.ng@sheffield.ac.uk

tively. Because each recession phase implies an existing glacier population, the portrayed sequence also demonstrates two waxing and waning cycles of alpine glaciation. The formation of underlying VFFs does not fully document the evolutionary history of lobate debris aprons and lineated valley fills, only a sample of which have been dated in our study.

**Examination of anomalous age findings**

As noted in the text, our age estimates show SGLF aggregates 10, 7, 17 and 28 to be older than their underlying VFFs (Table 1; Figure 5A), opposite to what the observed superposition of SGLFs on VFFs implies. To query these 'anomalous' findings, we revisited the respective landforms to check whether they are unusual in some way or have unique geomorphological characteristics or unique resurfacing histories that may explain the anomalies; we checked their identification and mapping also. The VFF ages in all four cases are $< 60$ Ma—at the young end of our set of VFF ages (up to $\sim$500 Ma). Conceivably, 'special' resurfacing events (e.g. burial by lava flow or other deposits) may have occurred on the VFFs to make their surfaces younger than they should be, while not affecting the SGLFs. Note, however, that in order for a data point in Figure 5A to be anomalous (left of the 1:1 line) its VFF age must be young, and a young VFF age does not prove it has been biased and misrepresents the true age (three of the four VFF ages in question fall well within the spread of younger VFFs ages in the R1 cluster in Figure 5A). Separately, one could look for reasons that biased the SGLF ages upward, although we cannot imagine what the relevant processes or histories would be.

Figure S36 locates the four sites and shows their CTX imagery. They span the Deuteronilus and Protonilus Mensae regions without any obvious spatial clustering or systematic contextual or locational attributes (e.g. whether the underlying VFF is a LDA or LVF; whether or not a SGLF 'flows' from a mesa) that distinguish them from other SGLF sites in our study (Figure 3), which were also examined for comparison. The presentation in Figure S36 of the four anomalous sites from west to east matches their order of descending SGLF aggregate ages, but this seems coincidental because other SGLF aggregates do not show such a consistent transgression (Movie S1). A lack of clear distinction can also be said for the planforms of the SGLFs and VFFs at the four sites, as well as their surface features and textures, all of which fall within the range of variations seen at other sites. None of the SGLFs/VFFs appear to have been modified by extraneous or unexpected surface/resurfacing processes; not surprisingly, the visible abundances of craters on them are broadly consistent with the crater counts used in their dating. In short, we found nothing geomorphologically unusual or significant that makes them stand out from the other 31 SGLF aggregate-VFF pairs in our study.

Dating uncertainty offers another potential explanation for the anomalous findings, as the errors on the model ages in Figure 5A can influence how confidently we can say which side of the 1:1 line a given plotted point falls. In the four anomalous cases, the age-error magnitudes and how these relate to the fitting of the respective CSFDs (Figure S36, bottom) are both worth considering. In all four cases the VFF ages seem robust, with relatively low uncertainty of no more than $\pm 11$ Ma, due to a reasonable abundance of craters on the fitted CSFD limbs (12 to 35 craters, Table 1) for the ages determined. In contrast, for the SGLF aggregates, the low numbers of craters on their fitted CSFD limbs (3 to 12 craters, Table 1) cause substantial dating uncertainty, especially for aggregates 10, 7 and 17 where the age errors are $\pm$ tens of Ma (Figure S36). In fact, there is additional uncertainty (not reflected by error bars) for aggregates 10 and 28 because their CSFDs show less well defined limbs for dating (Figure S36): the fitted isochron may be misplaced. These considerations suggest that the true ages of the SGLF aggregates may be considerably less than estimated, so much that the anomalous points in Figure 5A can be relocated to right of the 1:1 line (aggregate 17 is the least controversial because its point lies close to the line and its SGLF age error is large). Given the fruitless geomorphological exploration above, we prefer this way of resolving the anomalies. Notice we are not selectively invoking age errors only to treat this problem—dating uncertainty matters for the other data points in Figure 5A. Notably, the “R2” data points right of the 1:1 line (and lying near it) have large errors in their SGLF aggregate age and sometimes their underlying VFF age. However, shifting them to their error limits cannot move them convincingly into the area left of the 1:1 line to create anomalies. Age uncertainty has also been taken into account in our $k$-means clustering analysis of the SGLF aggregate ages in Section 3.2.

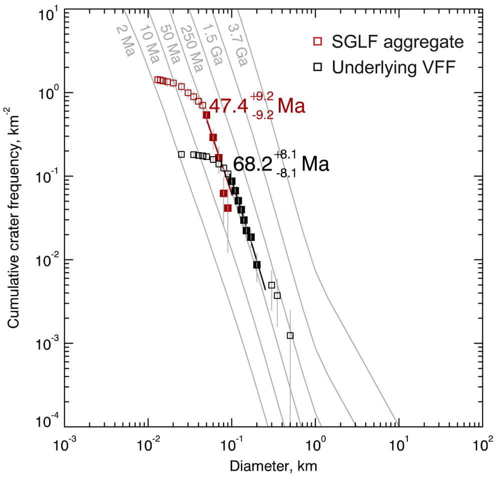


**Figure S1. Impact crater size-frequency distributions of SGLF aggregate 1 and its underlying VFF**. Data points are derived from crater counts on CTX imagery (Table 2 of the online data repository for this paper). Grey curves outline the isochron system. Ages are determined by isochron fitting (red and black lines) to the filled data points; the corresponding crater-diameter ranges are documented in Table 1.

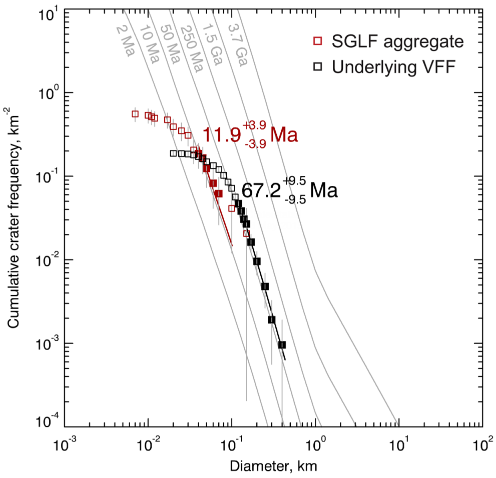


**Figure S2. Aggregate 2**. See Figure S1 caption.

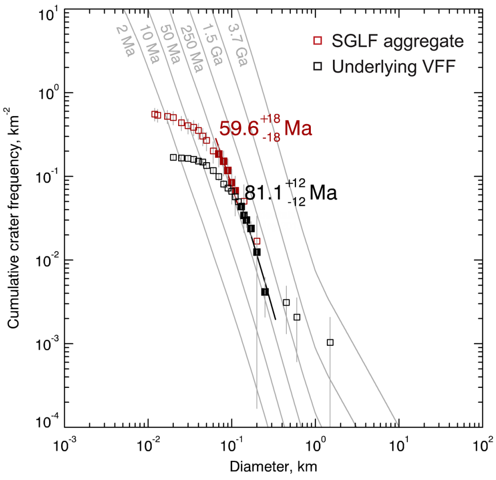


**Figure S3. Aggregate 3**. See Figure S1 caption.

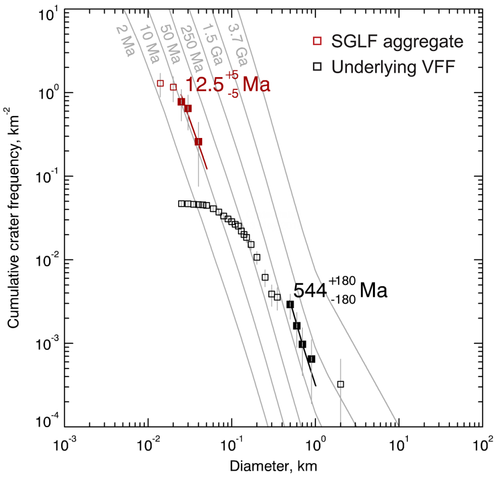


**Figure S4. Aggregate 4**. See Figure S1 caption.

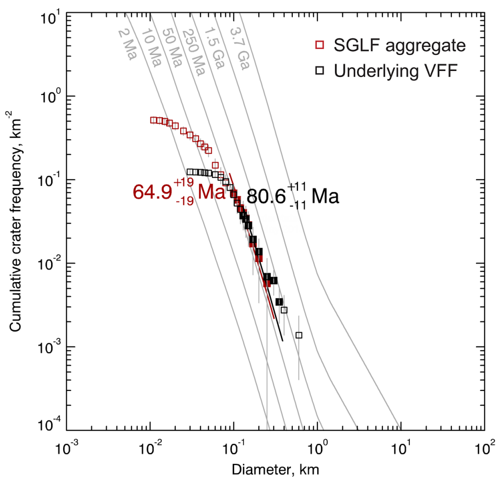


**Figure S5.** **Aggregate 5**. See Figure S1 caption.

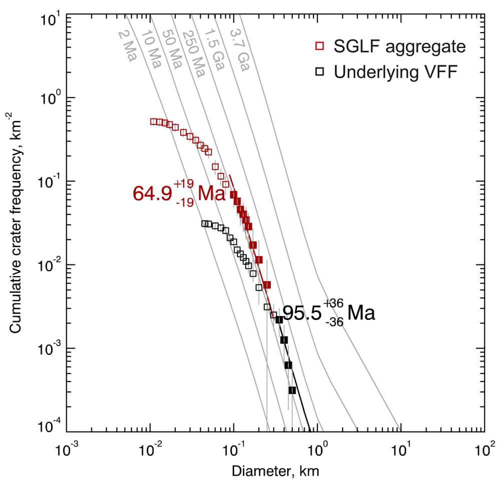


**Figure S6.** **Aggregate 6**. See Figure S1 caption.

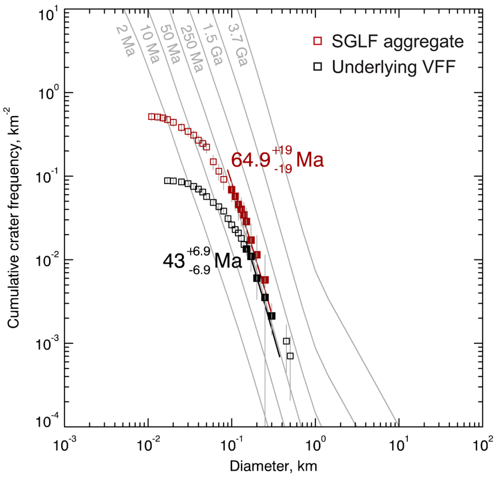


**Figure S7. Aggregate 7**. See Figure S1 caption.

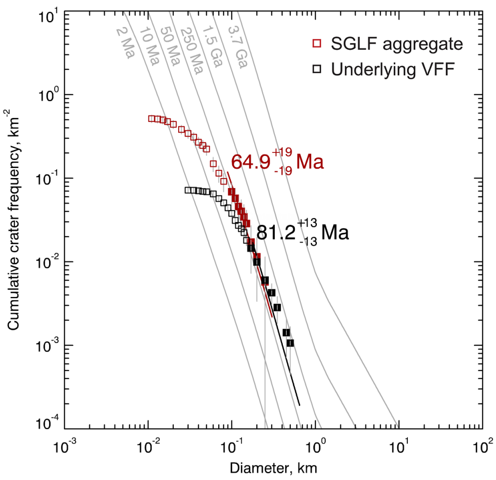


**Figure S8. Aggregate 8**. See Figure S1 caption.

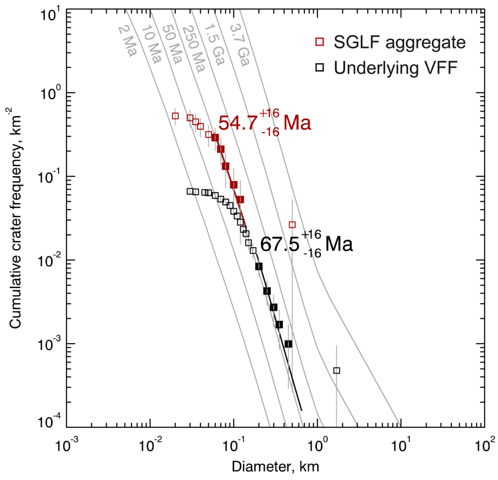


**Figure S9. Aggregate 9**. See Figure S1 caption.

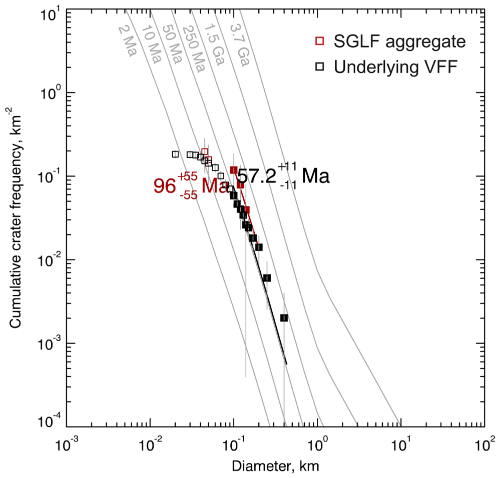


**Figure S10. Aggregate 10**. See Figure S1 caption.

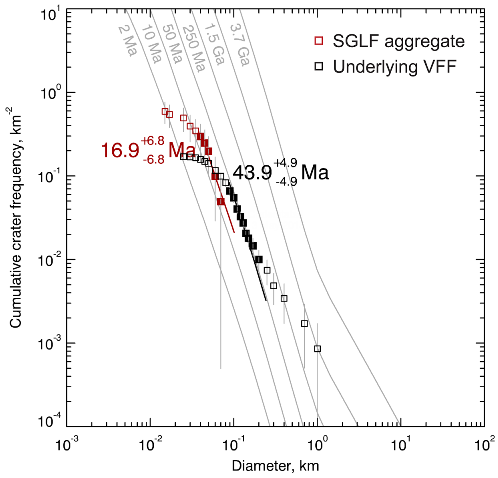


**Figure S11. Aggregate 11**. See Figure S1 caption.

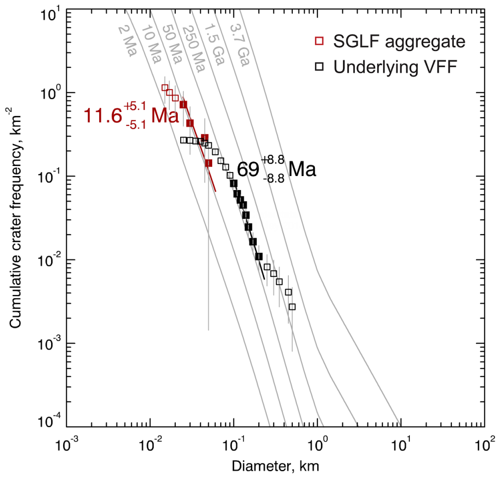


**Figure S12. Aggregate 12**. See Figure S1 caption.

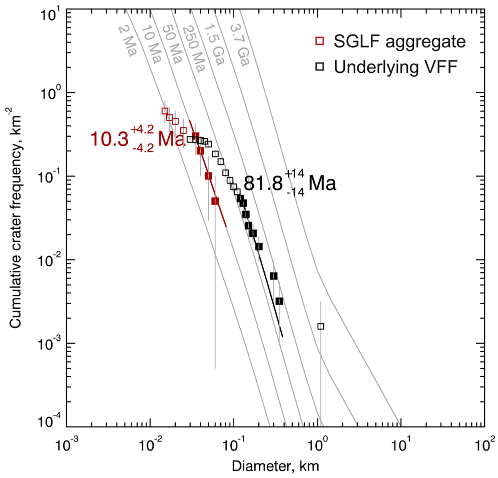


**Figure S13.** **Aggregate 13**. See Figure S1 caption.

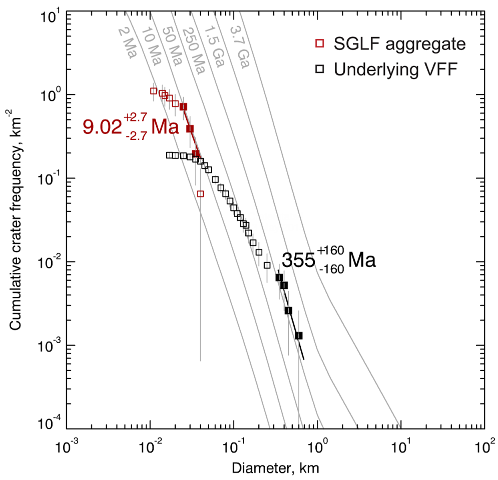


**Figure S14.** **Aggregate 14**. See Figure S1 caption.

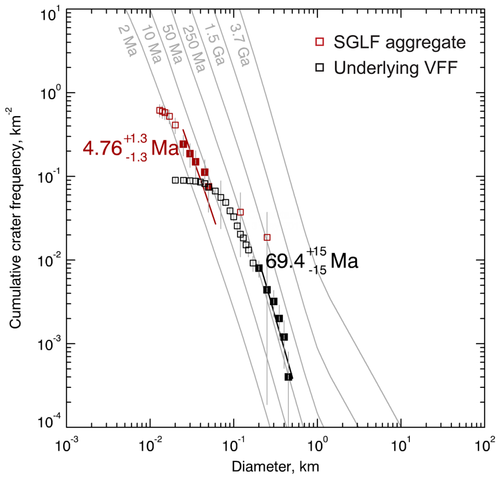


**Figure S15. Aggregate 15**. See Figure S1 caption.

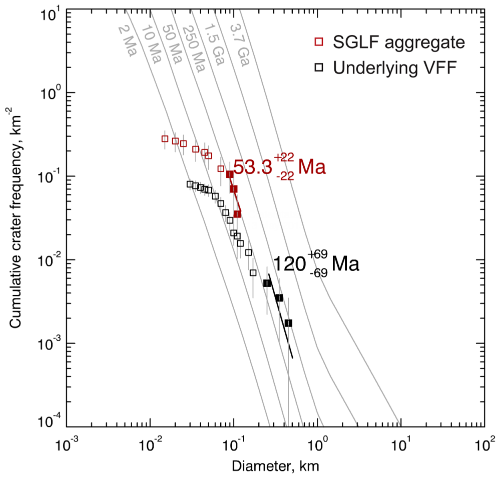


**Figure S16. Aggregate 16**. See Figure S1 caption.

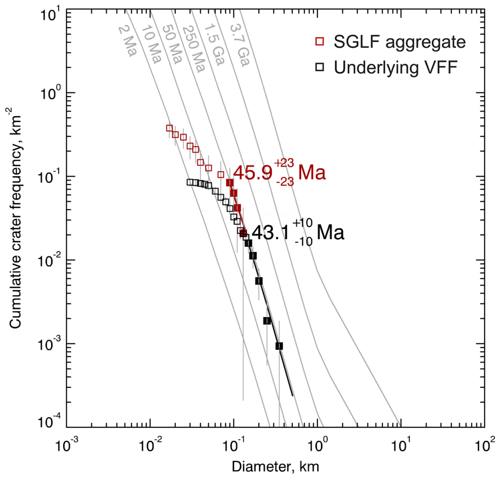


**Figure S17.** **Aggregate 17**. See Figure S1 caption.

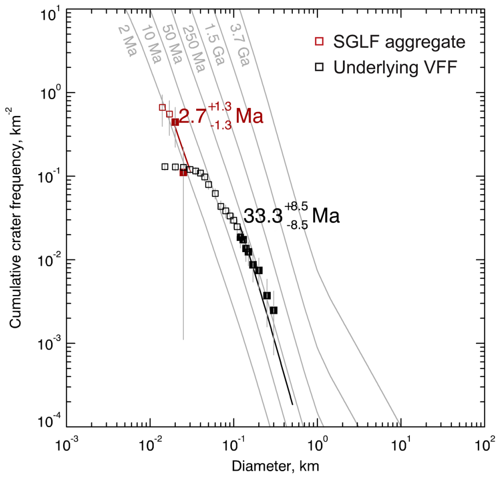


**Figure S18.** **Aggregate 18**. See Figure S1 caption.

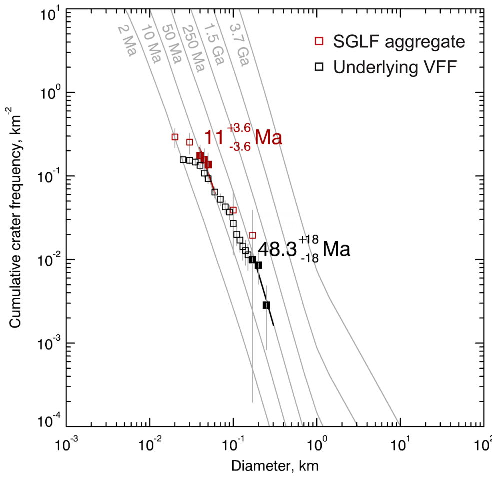


**Figure S19.** **Aggregate 19**. See Figure S1 caption.

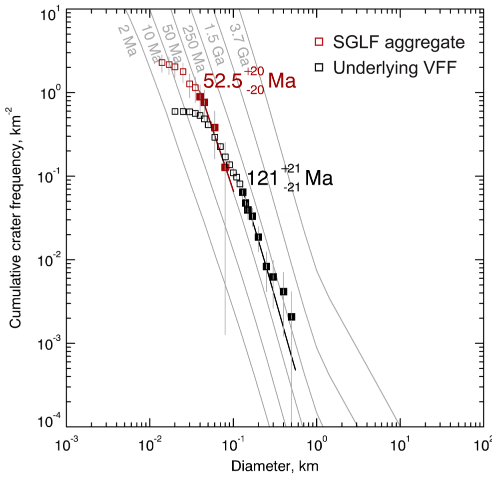


**Figure S20.** **Aggregate 20**. See Figure S1 caption.

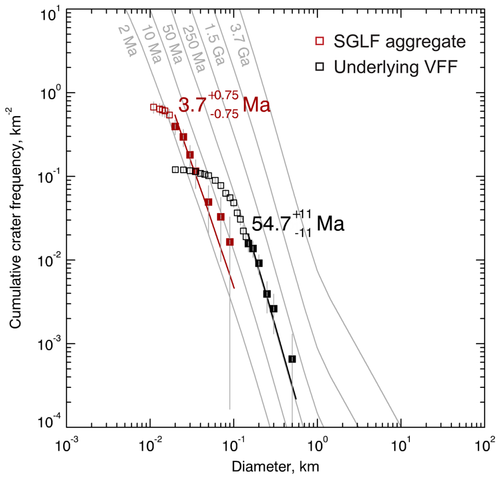


**Figure S21. Aggregate 21**. See Figure S1 caption.

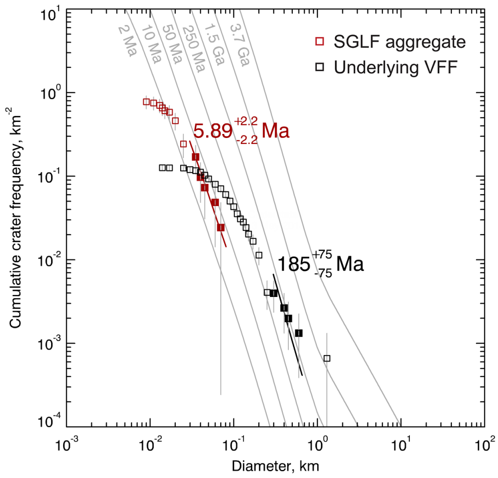


**Figure S22. Aggregate 22**. See Figure S1 caption.

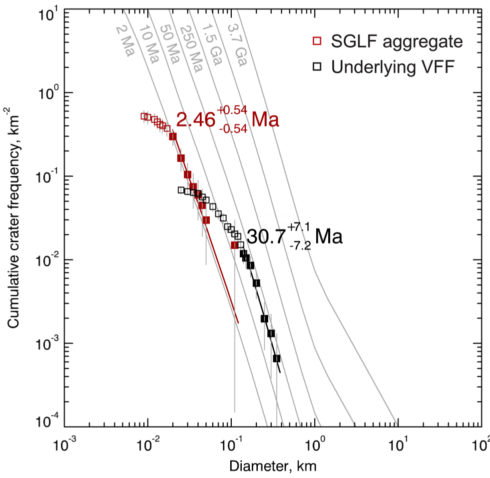


**Figure S23. Aggregate 23**. See Figure S1 caption.

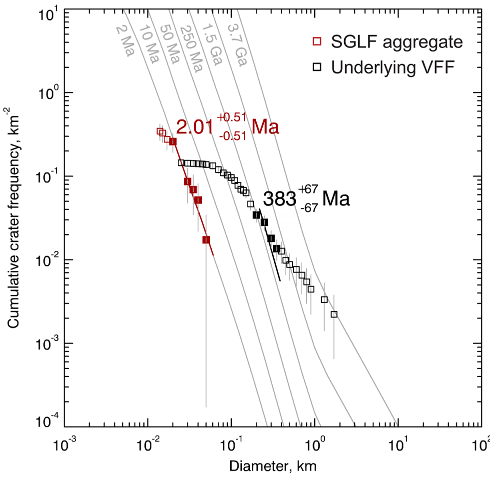


**Figure S24. Aggregate 24**. See Figure S1 caption.

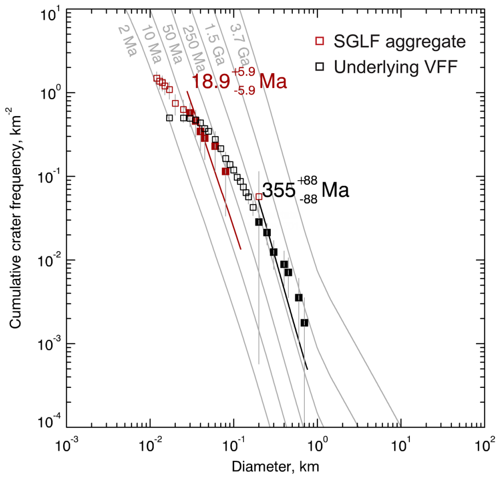


**Figure S25. Aggregate 25**. See Figure S1 caption.

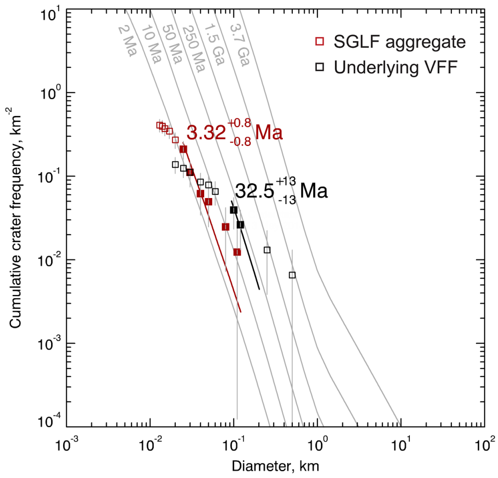


**Figure S26. Aggregate 26**. See Figure S1 caption.

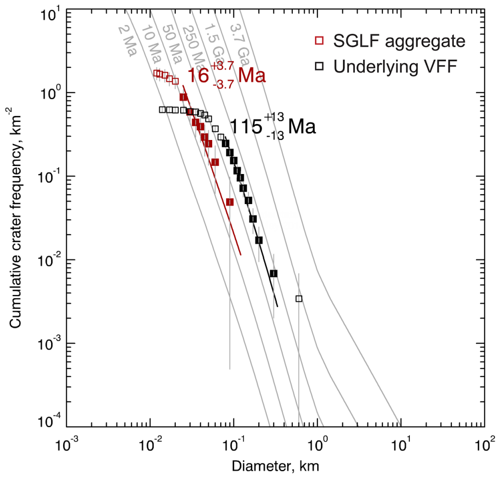


**Figure S27.** **Aggregate 27**. See Figure S1 caption.

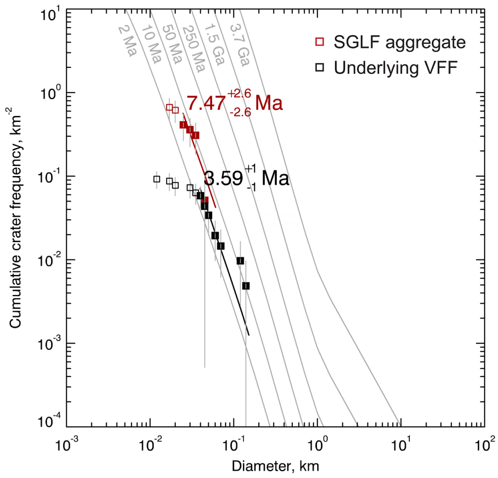


**Figure S28.** **Aggregate 28**. See Figure S1 caption.

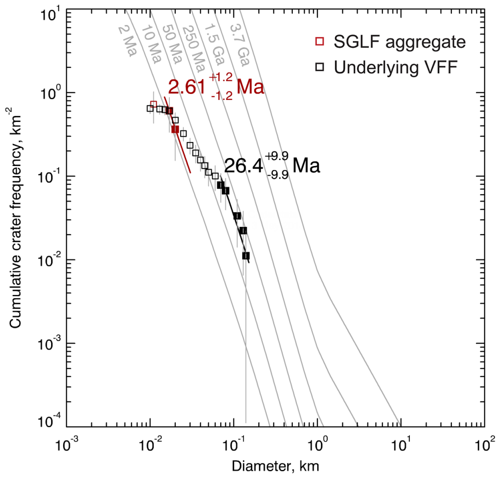


**Figure S29.** **Aggregate 29**. See Figure S1 caption.

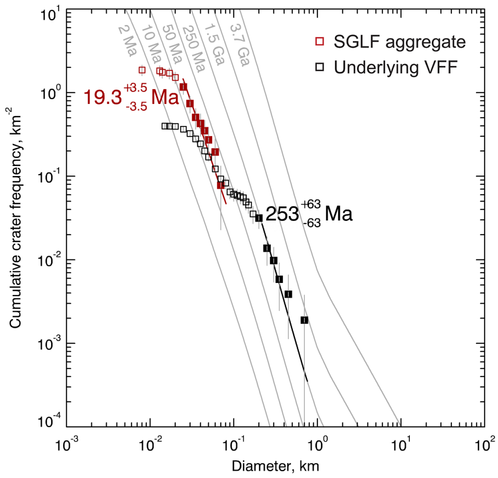


**Figure S30.** **Aggregate 30**. See Figure S1 caption.

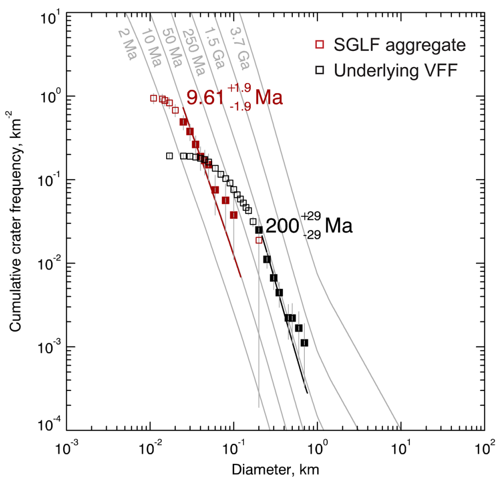


**Figure S31.** **Aggregate 31**. See Figure S1 caption.

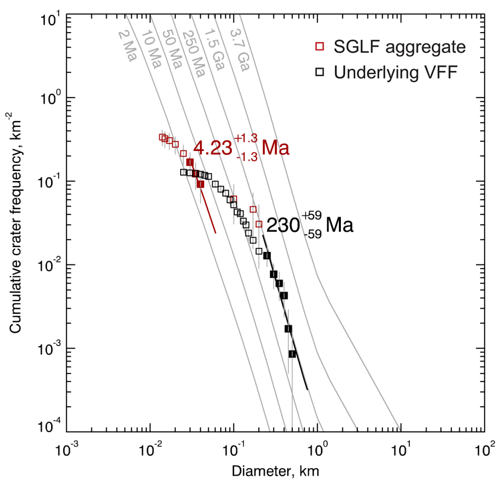


**Figure S32.** **Aggregate 32**. See Figure S1 caption.

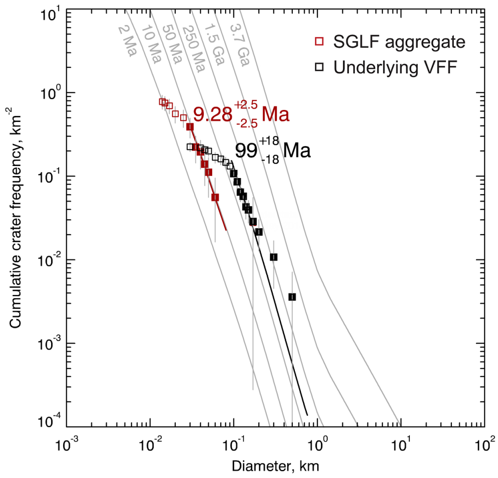


**Figure S33.** **Aggregate 33**. See Figure S1 caption.

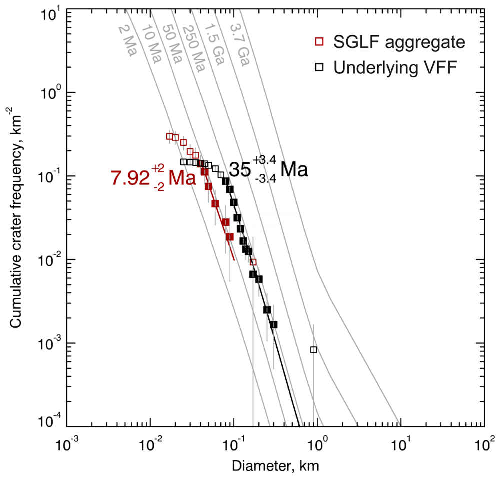


**Figure S34.** **Aggregate 34**. See Figure S1 caption.

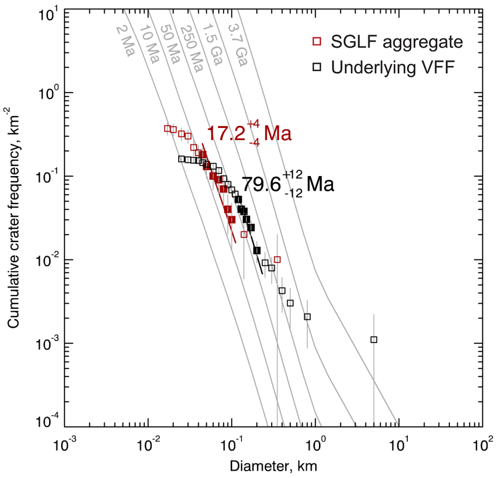


**Figure S35. Aggregate 35**. See Figure S1 caption.

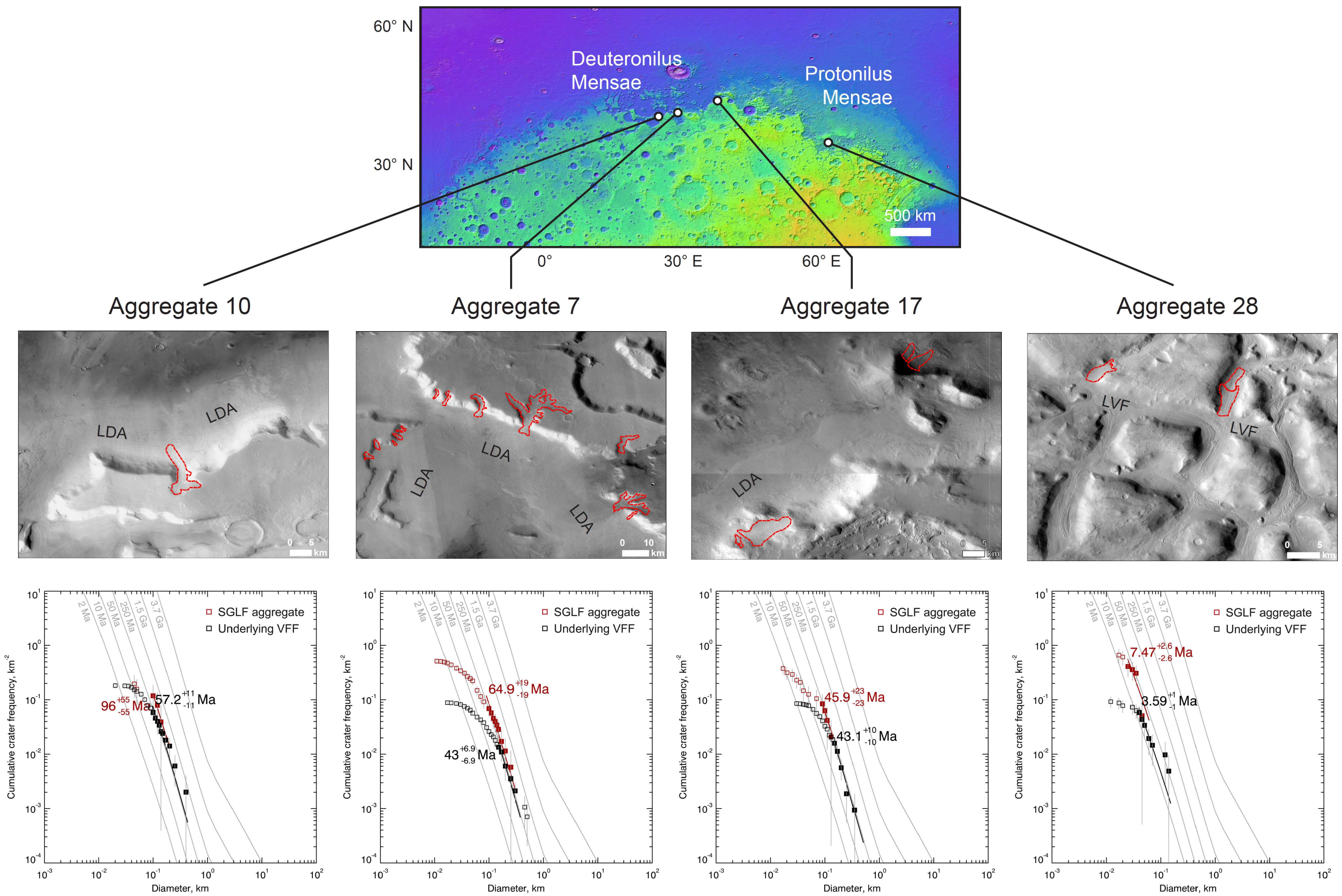


**Figure S36. Location, landforms and dating of four sites that yielded 'anomalous' age findings.** The middle panels display mosaicked CTX imagery (Dickson et al., 2018) of the areas around SGLF aggregates 10, 7, 17, 28 (outlined in red) and their underlying VFFs (labelled LDA or LVF). The bottom panels show the corresponding crater size-frequency distributions and fitted isochrons. The MOLA DEM at the top locates the four sites.

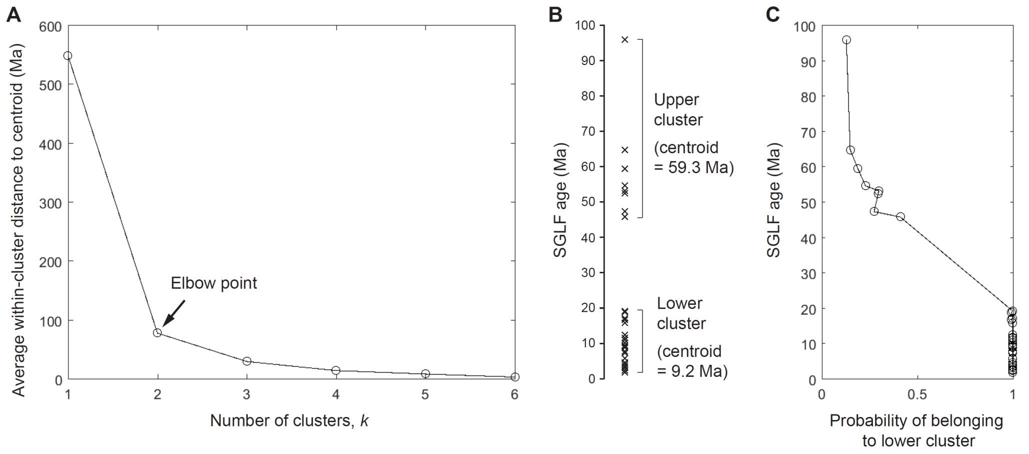


**Figure S37. Results of $k$-means clustering with the SGLF ages, with $k$ being the number of clusters.** (**A**) Average distance between each age and the centroid of the cluster to which the age belongs after k-means optimisation, for different $k$ from 1 to 6. The 'elbow' at $k = 2$ indicates two clusters as the best description of the age data. (**B**) Optimal clustering of the ages when $k$ =2 (and cluster centroids) on the age axis. (**C**) The probability of each age belonging to the lower cluster in panel B, computed from a Monte-Carlo simulation of $10^6$ runs. In each run, each SGLF age is first perturbed randomly based on its age uncertainty (we assume that each age error bar in Figure 5a approximates $1\sigma$ of a normal distribution in age) before $k$-means optimisation with $k = 2$. Different runs thus cluster the ages differently. The probability displayed is calculated from the frequency of an age being assigned to the lower cluster after the random perturbations. Low probability for the ages above 45 Ma shows that they are unlikely to belong to that cluster; however, their probability values are not very near zero because those ages are accompanied by large uncertainty (Figure 5a). Note that omitting the SGLF age value at 96 Ma changes all of these results negligibly. We exclude this outlier age in the paper when reporting the age ranges of the two clusters (2-20 Ma, 45-65 Ma)

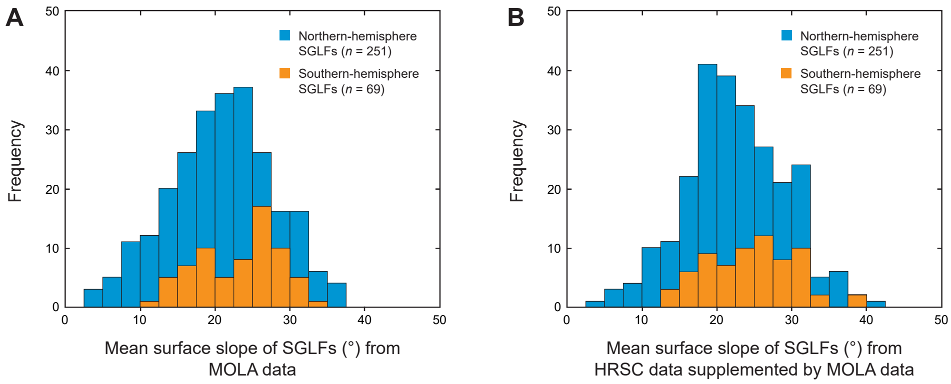


**Figure S38. Histograms of mean surface slope of the 320 SGLFs in our inventory.** (**A**) Results from MOLA (Mars Orbiter Laser Altimeter) digital elevation model. (**B**) Results from HRSC (High-Resolution Stereo Camera) digital elevation model, supplemented by MOLA data where HRSC data are not available for a SGLF. Comparison with Figure 5C shows that our slope-based conclusions are not sensitive to the choice of input elevation data.

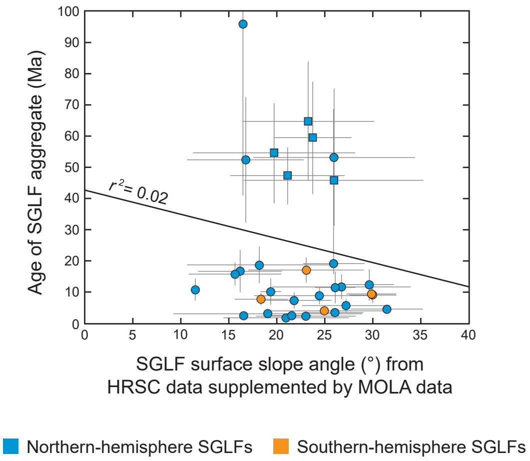


**Figure S39. Age of each aggregate of SGLFs versus their mean surface slope derived from HRSC (High-Resolution Stereo Camera) digital elevation data.** This figure is a version of Figure 5C based on alternative data source. HRSC data are supplemented by MOLA data where they are not available for a SGLF. Solid line depicts regression through data. Square symbols identify those SGLF aggregates in recession phase R2 (aggregates 1, 3, 5–9 and 17) whose ages are similar to their underlying VFF ages, as in Figure 5.

**Table S1. Statistical summary of the morphometry of 320 superposed glacier like forms (SGLFs) and 1309 glacier-like forms (GLFs).** The GLF results derive from Souness et al. (2012). GLFs are the lowest-order viscous flow feature (VFF). SGLFs are a subset of the GLF population, and these results confirm that they are morphometrically similar to GLFs.

| VFF type | | Length (km) | Width (km) | Area ($km^2$) | Elevation (m)† |
|---|---|---|---|---|---|
| GLF ($n$=1300) | Mean | 4.66 | 1.27 | 7.61 | -366 |
| | Standard deviation | 3.37 | 0.93 | 13.4 | 1954 |
| SGLF ($n$=320) | Mean | 5.77 | 1.63 | 8.43 | -1365 |
| | Standard deviation | 4.03 | 3.61 | 14.3 | 1375 |

† Elevation measured above Mars's topographic datum.

## References

Dickson, J., Kerber, L., Fassett, C., & Ehlman, B. (2018). A global, blended CTX mosaic of Mars with vectorized seam mapping: a new mosaicking pipeline using principles of non-destructive image editing. In *49th lunar and planetary science conference.*

Souness, C., Hubbard, B., Milliken, R., & Quincey, D. (2012). An inventory and population-scale analysis of martian glacier-like forms. *Icarus*, *217*(1), 243–255. doi: 10.1016/j.icarus.2011.10.020